

Ultrasensitive Ag-coated TiO<sub>2</sub> nanotube arrays for flexible SERS-based optofluidic devices

*Original*

Ultrasensitive Ag-coated TiO<sub>2</sub> nanotube arrays for flexible SERS-based optofluidic devices / Lamberti, A., Virga, A., Chiado', A., Chiodoni, A., Bejtka, K., Rivolo, P., Giorgis, F.. - In: JOURNAL OF MATERIALS CHEMISTRY. C. - ISSN 2050-7526. - STAMPA. - 3:26(2015), pp. 6868-6875. [10.1039/c5tc01154j]

*Availability:*

This version is available at: 11583/2619251 since: 2021-03-30T16:34:10Z

*Publisher:*

Royal Society of Chemistry

*Published*

DOI:10.1039/c5tc01154j

*Terms of use:*

This article is made available under terms and conditions as specified in the corresponding bibliographic description in the repository

*Publisher copyright*

GENERICO -- per es. Nature : semplice rinvio dal preprint/submitted, o postprint/AAM [ex default]

The original publication is available at

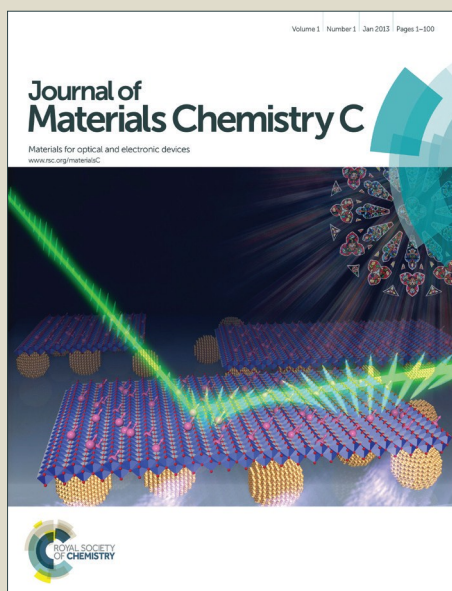
<http://pubs.rsc.org.ezproxy.biblio.polito.it/en/Content/ArticleLanding/2015/TC/C5TC01154J#!divAbstract/>

<http://dx.doi.org/10.1039/c5tc01154j>.

(Article begins on next page)

# Journal of Materials Chemistry C

Accepted Manuscript



This is an *Accepted Manuscript*, which has been through the Royal Society of Chemistry peer review process and has been accepted for publication.

*Accepted Manuscripts* are published online shortly after acceptance, before technical editing, formatting and proof reading. Using this free service, authors can make their results available to the community, in citable form, before we publish the edited article. We will replace this *Accepted Manuscript* with the edited and formatted *Advance Article* as soon as it is available.

You can find more information about *Accepted Manuscripts* in the [Information for Authors](#).

Please note that technical editing may introduce minor changes to the text and/or graphics, which may alter content. The journal's standard [Terms & Conditions](#) and the [Ethical guidelines](#) still apply. In no event shall the Royal Society of Chemistry be held responsible for any errors or omissions in this *Accepted Manuscript* or any consequences arising from the use of any information it contains.



## Ultrasensitive Ag-coated TiO<sub>2</sub> nanotube array for flexible SERS-based optofluidic devices†

Andrea Lamberti,<sup>a\*</sup> Alessandro Virga,<sup>a</sup> Alessandro Chiadò,<sup>a</sup> Angelica Chiodoni,<sup>b</sup> Katarzyna Bejtka,<sup>b</sup> Paola Rivolo,<sup>a</sup> and Fabrizio Giorgis<sup>a,b\*</sup>

Received 00th January 20xx,  
Accepted 00th January 20xx

DOI: 10.1039/x0xx00000x

[www.rsc.org/](http://www.rsc.org/)

In this study, a novel SERS sensor has been developed for repeatable detection of organic molecules and biological assays. Vertically oriented Titania nanotubes arrays (TiO<sub>2</sub> NT) were grown by ultra-fast anodic oxidation of flexible titanium foils and then decorated with Ag nanoparticles (NPs) through d.c. sputtering deposition at room temperature. A parametric study was carried out taking into account the effect of sputtering parameters on the Ag NPs arrangements onto NTs surface. The structure morphology was investigated by means of scanning and transmission electron microscopies, evidencing the formation of hexagonal close-packed TiO<sub>2</sub> NTs coated with Ag nanoparticles showing tunable diameter and distribution. The substrates were employed into a SERS optofluidic device, consisting in a polydimethylsiloxane cover irreversibly sealed to the silvered TiO<sub>2</sub> NTs, able to detect Rhodamine molecules in ethanol over a wide range of concentrations down to 10<sup>-14</sup> M, taking advantage of both electromagnetic and chemical enhancements. In order to evaluate the performances of the SERS substrates in terms of biosensing, an optimized protocol for the immobilization of oligonucleotide probes on the metal-dielectric surfaces was developed for verifying the hybridization events.

### Introduction

Surface-enhanced Raman Spectroscopy (SERS) is a label-free detection method able to provide high sensitivity offering remarkable potential for biomolecular and chemical sensing.<sup>1-3</sup> Typical SERS active substrates are constituted by noble metals (Au, Ag, Cu, Pt) in the form of roughened surfaces, nanoparticle aggregates or arrayed elements.<sup>4-8</sup> From the application point of view, sensitivity, stability and reproducibility are key issues for SERS substrates. In order to optimize these features, the physical phenomena underlying SERS effect should be taken into account. There are two contribution to SERS enhancement: the electromagnetic (EM) enhancement linked to surface plasmon resonances and the so-called chemical enhancement due to charge transfer (CT) mechanisms. The former arises from the interaction of the exciting laser wavelength with the metal conduction band electrons in terms of localized surface plasmon excitation, leading to strong electromagnetic near fields associated to hot spots among adjacent metal surfaces. When these fields interact with a molecule adsorbed onto the metal surface hot spot, huge enhancements can be observed in the collected Raman signal.<sup>9</sup> The latter can be

attributed to charge transfer induced by the molecule-metal interaction: in certain favorable energetic conditions electrons can be transferred between the molecule and the metal, involving a vibrational level of the adsorbed analyte yielding a moderate Raman enhancement.<sup>10,11</sup> The synergy of electromagnetic and chemical enhancement can make SERS a sensitive technique allowing vibrational spectra detection from individual molecules.<sup>12,13</sup>

In addition to noble metals, semiconductors and transition metal-oxides have emerged as potential SERS-active substrates.<sup>14</sup> In particular, GaP nanoparticles (NPs)<sup>15</sup>, InAs/GaAs quantum dots<sup>16</sup>, Si and Ge nanowires/nanotubes<sup>17</sup> are representative examples of SERS substrates based on semiconductor nanostructures, while ZnO nanocrystals<sup>18</sup>, NiO<sup>19</sup>, Cu<sub>2</sub>O<sup>20</sup> and TiO<sub>2</sub><sup>21</sup> flat surfaces and nanostructures exhibited SERS effects on the metal-oxide side, showing noticeable SERS effect in absence of plasmonic enhancement, taking advantage of CT mechanisms<sup>22</sup> or total internal reflection/multiple light scattering.<sup>23</sup>

Combining metal-oxide nanostructures (such as TiO<sub>2</sub> nanotubes, NTs) and Ag/Au NPs it is possible to obtain a synergic effect of EM and CT enhancements (see Figure 1), exploiting also the high surface area to increase the amount of adsorbed molecules. Recently, following this concept several composites were investigated as SERS active substrate, such as ZnO/Si arrays decorated by Au nanoparticles<sup>24</sup> Au coated ZnO nanorods,<sup>25</sup> Ag decorated ZnO nanorods<sup>26</sup>, Au coated ZnO nanowires<sup>27</sup>, Ag decorated porous Al<sub>2</sub>O<sub>3</sub><sup>28</sup>, TiO<sub>2</sub> nanofibers decorated by Ag nanoparticles<sup>29</sup>, TiO<sub>2</sub>-coated silver nanowire<sup>30</sup>, Au coated TiO<sub>2</sub> nanotubes (NTs)<sup>31</sup> and Ag

<sup>a</sup> Department of Applied Science and Technology, Politecnico di Torino, C.so Duca degli Abruzzi 24 10129, Torino, ITALY.

<sup>b</sup> Istituto Italiano di Tecnologia, Center for Space Human Robotics, C.so Trento 21 10129, Torino, ITALY.

\* corresponding authors: A. Lamberti, [andrea.lamberti@polito.it](mailto:andrea.lamberti@polito.it)

F. Giorgis, [fabrizio.giorgis@polito.it](mailto:fabrizio.giorgis@polito.it)

†Electronic Supplementary Information (ESI) available. See

DOI: 10.1039/x0xx00000x

decorated TiO<sub>2</sub> nanorods and nanopore arrays<sup>32</sup> showing superior SERS capability and interesting smart properties such as photocatalytic degradation of probe molecule aimed to recycle the substrate.

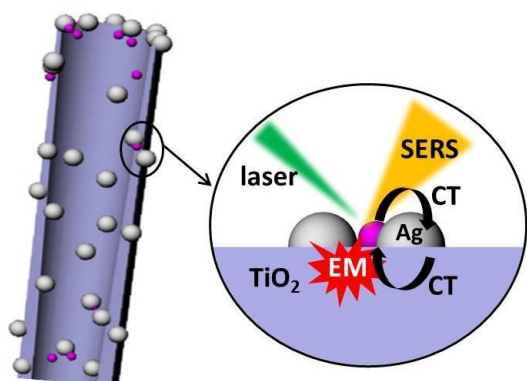


Figure 1. 3D scheme of the synergistic effect of electromagnetic and chemical enhancement obtainable coupling a TiO<sub>2</sub> metal-oxide nanostructure with Ag nanoparticles.

In this work, we discuss an easy and low cost method for the fabrication of SERS active substrates based on TiO<sub>2</sub> NTs decorated with Ag NPs, showing very low Limit of Detection (LOD) on Rhodamine 6G used as a probe molecule. Differently from the metal-dielectric nanostructures before cited, we present and discuss microfluidic devices integrating such kind of SERS-active substrates. The devices can be mounted on a microscope stage of a Raman spectrophotometer operating in backscattering configuration. Finally, in order to evaluate the performances of silvered TiO<sub>2</sub> SERS substrates in terms of biosensing, an optimized protocol for the immobilization of oligonucleotides probes on the metal-dielectric surfaces is developed, reporting the Raman detection of a model alkylthiol-capped DNA oligo strand and the hybridization of its complementary sequence.

## Experimental

### TiO<sub>2</sub> nanotubes growth and decoration with Ag nanoparticles.

Titania nanotube arrays were grown by an anodic oxidation of Ti foil (125 μm thick, 99.6% purity, Goodfellow) in an electrolytic solution made of 0.5 wt% NH<sub>4</sub>F (98%, Sigma Aldrich) and 2.5 wt% deionized water in ethylene glycol (99.5%, Sigma Aldrich). The process has been described in details elsewhere.<sup>33-35</sup> Briefly the anodization was performed in potentiostatic configuration applying 60 V for 10 min in a two-electrode electrochemical cell under continuous stirring in ambient environment. The sample were then annealed at 450°C for 1 hour in air to crystallized them into anatase phase (since the as grown NTs are amorphous<sup>35</sup>).

Ag nanoparticles were deposited by d.c. sputtering at room temperature in Ar atmosphere (Q150T-ES, Quorum Technologies) using a sputtering current of 40 mA for times ranging between 30 and 90 seconds.

### Fabrication of the optofluidic device.

Patterned NTs were fabricated by easy tape lithography followed by anodic oxidation and Ag sputtering deposition for 30 second (optimized sample). Polyimide adhesive tape was manually aligned and bonded to the clean Ti foil in order protect the Ti surface from oxidation outside from the desired geometry (NTs growing area equal to 10 × 0.2 mm<sup>2</sup>). Figure S1a in the ESI clearly depicts the patterning process.

Concerning the fabrication of the microfluidic device, the PDMS mixture (10:1 oligomer:curing agent ratio) was casted into a dedicated mold with a straight microchannel (10 mm long × 0.3 mm wide × 0.05 mm thick) connected to two pillars (resulting in inlet and outlet wells in the replica). The microfluidic element was manually aligned and bonded onto patterned Ag/TiO<sub>2</sub> NTs substrate by means of the “stamp and stick” bonding.<sup>36</sup> In detail, a thin layer of PDMS mixture was spun on a glass slice and then selectively transferred to the microfluidic chip using a stamping process. The chip was then bonded to the PDMS substrate by thermal treatment at 70°C for 30 min.

### Characterization.

Optical reflectance of the Ag-coated TiO<sub>2</sub> NTs membrane was measured by a PerkinElmer LAMBDA 35 spectrophotometer in the wavelengths range 300-900 nm.

Scanning electron microscopy images of silvered TiO<sub>2</sub> samples were obtained using a Zeiss SUPRA 40 Field Emission Electron Microscope (FESEM).

The sample for the Transmission Electron Microscopy (TEM) characterization has been prepared in cross-section via a standard lift out technique, by using a Focused Ion Beam (FIB, Zeiss Dual Beam Auriga) operated at 30kV. A final cleaning step using a FIB voltage of 2kV was also performed. TEM investigation was carried out with a FEI TECNAI F20ST microscope, equipped with an high angle anular dark field (HAADF) detector and with an EDAX SUTW Si-Li X-ray detector, operating at 200 KV, in scanning transmission electron microscopy (STEM) mode.

Raman spectra of Rhodamine 6G (R6G, diluted in ethanol at several molar concentrations) spotted on the SERS substrates were obtained by means of a Renishaw inVia Reflex micro-Raman spectrophotometer equipped with a cooled CCD camera. Samples were excited with an Ar-Kr laser source (wavelengths of 514.5 nm) through a microscope objective, providing a photon flux lower than 60 W/cm<sup>2</sup>. The spectral resolution and integration time were 3 cm<sup>-1</sup> and 15 s respectively. The presented Raman spectra were obtained after the subtraction of the baseline represented by the dye fluorescence.

The effect of Ag sputtering on TiO<sub>2</sub> NTs samples, at different deposition times, was investigated by Contact Angle measurements with an OCAH200 instrument (DataPhysics Instruments GmbH) equipped with a CCD camera and an automatic dosing system for the liquid. Deionized water, MilliQ grade (H<sub>2</sub>O) was used (droplet volume = 1.5 μL) for analysis, in ambient conditions, according to the sessile droplet method in

static mode. After acquisition of images, drop profiles were extracted and contact angles were calculated using the SCA20 software. For each kind of sample (three for each deposition time), three drops were dispensed at three different positions on the surface and the average value and standard deviation was obtained from the software.

### Biological protocol implementation

In order to develop a label-free-biosensing protocol by means of this new TiO<sub>2</sub> substrate, self-assembled monolayers of 5'-alkylthiol-capped DNA oligo strands on silver nanoparticles were prepared and used to detect a complementary RNA sequence. To simplify the experiment, two model oligos have been purchased (Sigma Aldrich): SH-C6-AAAAAA (the alkylthiol-capped DNA oligo strand, PolyA-SH), and UUUUUUU (the complementary RNA sequence, PolyU).

First of all, the PolyA-SH was reduced with DL-dithiothreitol (Sigma Aldrich), purified with IllustraMicroSpin G-25 columns (GE Healthcare) and diluted in TE-tween (10 mM Tris, 1 mM EDTA, 0.05 % tween20™, pH 7.5) to 100 μM. The PolyA-SH was then spotted (5 μL) on SERS substrates and incubated overnight at room temperature. Negative controls were as well incubated overnight in TE-tween without the PolyA-SH. After overnight incubation, the samples were washed thrice in TE-tween to remove non-specific binding. Afterwards, the PolyU, HPLC-purified by the vendor, was diluted in SSC 4x (Saline Sodium Citrate, 60 mM trisodium citrate, 600 mM NaCl, 0.1 % SDS, pH 7.5) to 100 μM, spotted on substrates (all the samples but the PolyA-SH controls), and incubated overnight to allow the hybridization. The samples were then washed thrice in SSC 1x (15 mM trisodium citrate, 150 mM NaCl, pH 7.5) to remove non-specific binding, and once in MilliQ water. The samples were then analyzed by SERS analysis.

## Results and discussion

### TiO<sub>2</sub> nanotubes grown and decoration with Ag nanoparticles.

Figure 2 shows the FESEM top view and cross section images of titania nanotubes after the electrochemical growth. The

length of TiO<sub>2</sub> NTs is 3.8 μm (Fig 2 a,b). The hexagonal close-packed TiO<sub>2</sub> NTs array (fig. 2c) is clearly visible, while the enlargement of the thickness of the pore walls toward the pore bottom has been evidenced in previous works.<sup>37-38</sup>

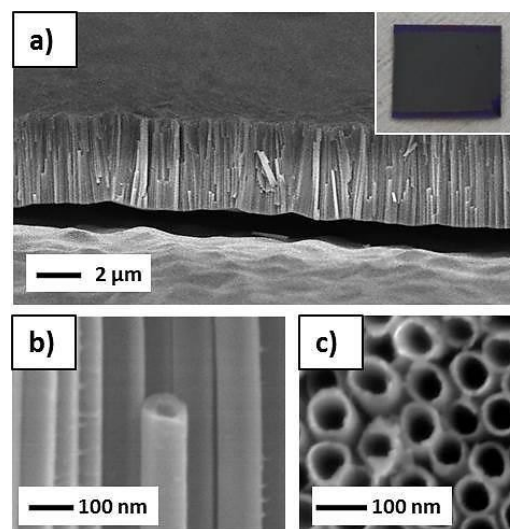


**Figure 2.** FESEM micrographs of the anodically grown TiO<sub>2</sub> NTs: cross-section (a, b) and top view (c). The inset in panel a) show a digital photographs of the annealed sample.

Figure 3 displays the morphology of Ag-TiO<sub>2</sub> NTs after different d.c. sputtering time ( $t_{\text{SPUT}}$ ). Compared with Figure 2, the surface of the samples is covered with silver nanoparticles on the top of titania nanotubes walls. Actually, despite of the regular distribution of TiO<sub>2</sub> NTs, the Ag synthesized particles do not consist of regular arrays. An analysis of FESEM images was performed by a self-made routine running on the MATLAB (The Mathworks Inc, Natick, MA, USA) platform in which SEM micrographs were partitioned into subimages and then segmented using an adaptive threshold. Each NP was approximated by a circular 'equivalent particle' having the same planar area. Following such a procedure, the particle sizes can be expressed in terms of the diameters of equivalent circular particles.

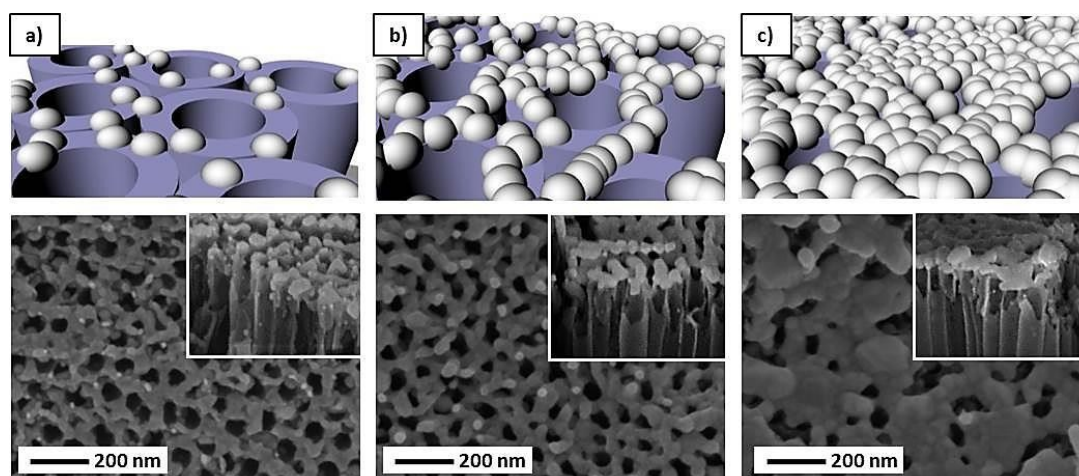


**Figure 3.** 3D schemes and FESEM images of the TiO<sub>2</sub> NT array decorated with Ag NPs by increasing the sputtering time: 30 s (a), 60s (b), 90 s (c).

We find that increasing the sputtering time, the average size of silver nanoparticles grows from  $63 \pm 15$  nm at  $t_{\text{SPUT}} = 30$  s (Figure 3a) to  $99 \pm 10$  nm at  $t_{\text{SPUT}} = 60$  s (Figure 3b). For longer sputtering time ( $t_{\text{SPUT}} = 90$  s), silver nanoparticles coalesce among them creating interconnected clusters covering the top-side of Ag-TiO<sub>2</sub> NTs as shown in Figure 2c.

The inset images in Figure 2 show the cross sections of Ag-TiO<sub>2</sub> NTs in which small NPs are clearly visible inside the inner walls of NTs (more evidenced by the TEM analysis discussed below).

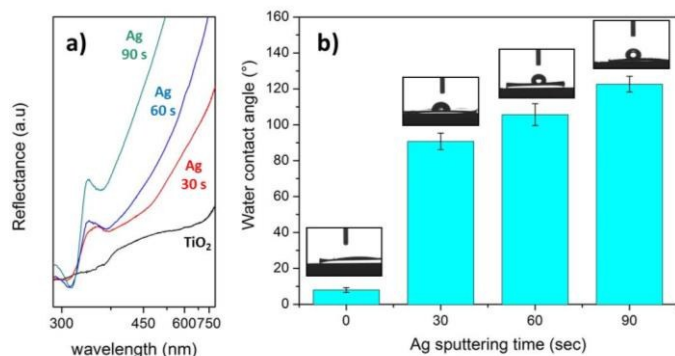


**Figure 4.** Optical spectra (a) and wetting properties (b) of TiO<sub>2</sub>NTs with and without Ag nanoparticles grown with several sputtering time.

Specular reflectance measurements have been performed on the samples characterized by FESEM in order to analyse the optical response of TiO<sub>2</sub> nanotubes decorated by Ag NPs with different morphology (i.e. sputtering times). Figure 4a shows the optical spectra. The bare TiO<sub>2</sub> nanotubes exhibit the typical TiO<sub>2</sub> spectrum due to the absorption edge assigned to the intrinsic transition from the valence band (VB) to the conduction band (CB) located at around 390 nm.<sup>39</sup>

The spectra of TiO<sub>2</sub>NTs coated with Ag nanoparticles show the appearance of dips corresponding to plasmon resonances attributed to enhanced absorption/scattering processes. For all the samples synthesized with different sputtering time it is possible to observe a specific dip around 310-320 nm due to the Ag bulk plasmon resonance,<sup>40</sup> while additional dips located in UV-visible wavelength range can be ascribed to either localized surface plasmons (LSP) coupled to individual particles or yielded by interparticles short-range interactions.

By increasing the sputtering time it is possible to observe a spectral blue-shift and narrowing of the plasmonic resonances. Theoretical and experimental analysis previously conducted on other substrates decorated by Ag/Au nanoparticles evidence a spectral shift of the plasmon resonances by changing the inter-particle gap and the average particle size. Indeed, the main plasmon resonance is subjected to a spectral blue-shift by increasing the inter-particle nano gap, while fixing the gap, the increase of the particle size induces a red-shift.<sup>41</sup>

In the present set of samples it is difficult to distinguish the contribution of nanoparticle size and inter-particle gaps since both are affected by the sputtering time; moreover larger sputtering time yields a marked nanoparticles coalescence. In particular, the sample subjected to 30 seconds of Ag sputtering shows a broad resonance within the range of 360-500 nm. Such a broad resonance could be ascribed to the distribution of NPs size and of the inter-particle gap.

Actually, the surface morphology observed by FESEM for the sample with the lower sputtering time (see Figure 3a) shows nanoparticles with size in the range 50-80 nm and a multimodal distribution of inter-particles gap ranging from very small gaps among adjacent nanoparticles 5-10 nm to larger gaps (20-50 nm) due to the TiO<sub>2</sub> nanotube inner hole.

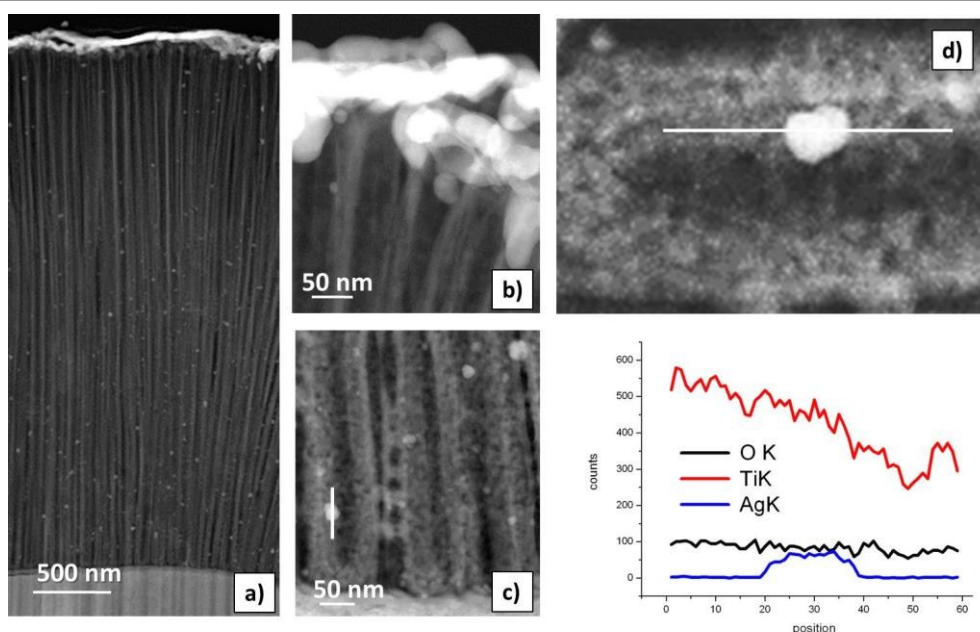


**Figure 5.** TEM images of the cross section of the TiO<sub>2</sub> NT sample with Ag sputtering time of 60 s. a) cross section, b) detail of the top, c) detail of the bottom, d) EDX line profile of an Ag particle in the bottom of the sample.

Moreover, beside the NPs morphology, the effect of the dielectric substrate ( $\text{TiO}_2$ ) on the LSP resonance energies must be taken into account, since they are subjected to a spectral red shift by increasing the dielectric constant of the hosting matrix.<sup>42</sup>

Increasing the sputtering time the nanoparticles start to coalesce on the nanotubes topside leading to interconnected Ag NPs clusters with increased thickness, weakening the influence of the dielectric substrate on the optical response of the Ag nanostructures (see Figure 3b-c). This morphology variation directly influences the optical reflectance showing a spectral shrinking as well as a blue-shift of the plasmon resonances down to 355 nm by increasing the Ag sputtering time up to 90s. The wettability of  $\text{TiO}_2$  NTs decorated with Ag nanoparticles was investigated by contact angle (CA) analysis (Figure 4b). The measured  $\text{H}_2\text{O}$  CA (WCA) increases by increasing the Ag  $t_{\text{SPUT}}$ . Actually, the bare  $\text{TiO}_2$  NT substrates show a highly hydrophilic behavior ( $\text{WCA} \cong 8^\circ$ ). A first abrupt CA increase is observed after a  $t_{\text{SPUT}}$  of 30s ( $\text{WCA} \cong 90^\circ$ ). An increase of surface hydrophobization ( $\text{WCA}$  ranging from  $110^\circ$  to  $120^\circ$ ) due to successive growth and coalescence of Ag nanostructures<sup>43</sup> is observed at higher  $t_{\text{SPUT}}$  (60 and 90 s).

Figure 5 reports the TEM characterization of the  $\text{TiO}_2$  NTs sample with 60s silver sputtering time. The measurements were performed in STEM imaging mode, by using an high angle annular dark field (HAADF) detector, to put the Z-contrast in evidence. In Figure 5a, the cross section of the sample is shown. Ag nanoparticles, with a random crystalline orientation (data not shown here), are characterized by sizes in the range of 5-25 nm, and are observed along all the length of  $\text{TiO}_2$  NTs, as shown in figures 5a-c. On the top-side, a layer of bigger NPs, with an average size of 100 nm are evidenced (Figure 5b), confirming the previously discussed FESEM characterization. Taking advantage of the Z-contrast enhanced by the HAADF detector, Ag particles distributed within the titania matrix (bright vs. dark regions) are well evidenced. In Figure 5d, an energy dispersive X-ray (EDX) line profile confirms the composition of a single Ag particle in the bottom of the sample, demonstrating also the synthesis of the Ag particles within the  $\text{TiO}_2$  NTs during the sputtering process.

#### SERS analysis and microfluidic device

The metal-dielectric nanostructures, here discussed, have been used as efficient SERS substrates for the detection of organic molecules and oligonucleotides. Indeed, Rhodamine 6G (R6G) diluted in ethanol at concentration ranging within  $10^{-5} \text{ M} - 10^{-15} \text{ M}$  has been used as a probe molecule.

Figure 6a shows the Raman spectra of R6G at limit of detection (LOD) for the silvered  $\text{TiO}_2$  NTs substrates discussed before.

The substrate synthesized with  $t_{\text{SPUT}} = 30\text{s}$  shows a LOD of  $10^{-14} \text{ M}$ , while much higher LOD was found for the other substrates ( $10^{-10} \text{ M}$  for  $t_{\text{SPUT}} = 60\text{s}$  and  $10^{-8} \text{ M}$  for  $t_{\text{SPUT}} = 90\text{s}$ ). These results are coherent with the reflectance spectra shown in Figure 4a. Actually, the substrate featured by the lowest LOD (among the lowest found in the literature on Raman detection of R6G<sup>44,45</sup>), is characterized by a broad plasmonic resonance covering the excitation/Raman emission wavelengths (excitation at  $\lambda_{\text{exc}} = 514.5 \text{ nm}$ ), while the LOD increases as the plasmonic dip is blue-shifted with respect to  $\lambda_{\text{exc}}$ . In summary, the best results has been obtained for excitation matching both the plasmonic resonance of the SERS substrate and the electronic resonance of the analyte (SERRS, Surface Enhanced Resonant Raman Scattering regime<sup>46</sup>).

Figure 6b shows SERRS spectra of R6G at several concentrations adsorbed on Ag- $\text{TiO}_2$  NT sample synthesized with Ag deposition time of 30s.

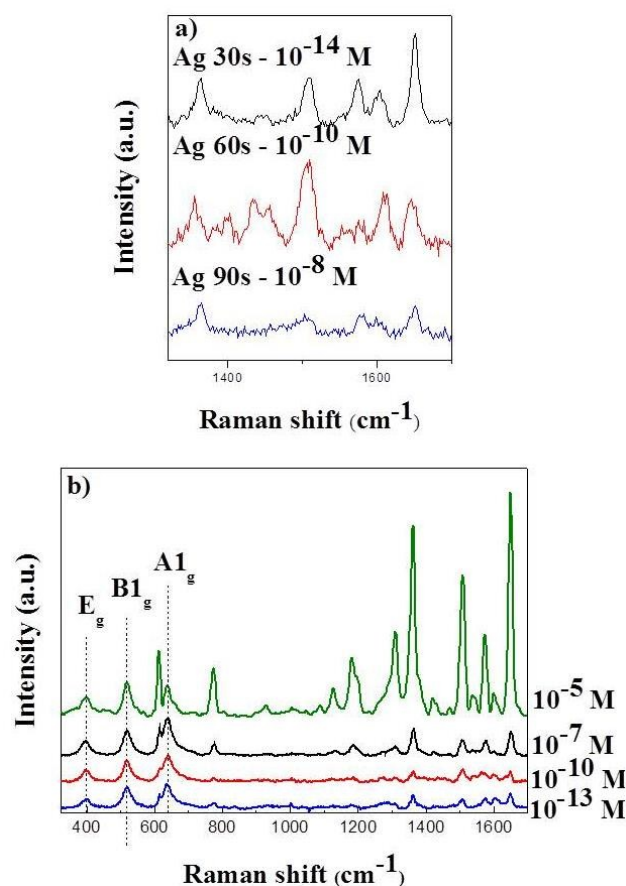


**Figure 6.** Raman spectra of  $\text{TiO}_2$  NTs showing the LOD of R6G for the different Ag sputtering times (a) and SERS enhancement at different R6G concentration for the most performing substrate (30 sec) (b).

The SERRS spectra show the typical modes related with C-C stretching in the xanthene ring at  $1650\text{ cm}^{-1}$ , C-C stretching in the phenyl ring at  $1574\text{ cm}^{-1}$ , C-C ring stretching in xanthene ring at  $1510\text{ cm}^{-1}$  and  $1362\text{ cm}^{-1}$ , hybrid mode regarding NHC<sub>2</sub>H<sub>5</sub> group and aromatic rings at  $1310\text{ cm}^{-1}$ , C-H in-plane bending in xanthene ring at  $1182\text{ cm}^{-1}$ , C-H in-plane bending in aromatic rings at  $1127\text{ cm}^{-1}$ , C-H out-of-plane bending at  $773$  and C-C in-plane bending in aromatic rings at  $612\text{ cm}^{-1}$ . At low wavenumbers, three peaks related with anatase crystalline Titania can be noticed at  $639$ ,  $518$  and  $399\text{ cm}^{-1}$ , which correspond to  $E_g$ ,  $B_{1g}$  and  $A_{1g}$  modes, respectively.<sup>47</sup> Moreover, it is worth to underline that the peculiar structure of these substrates can activate CT phenomena, also considering surface defects distributed within the TiO<sub>2</sub> NTs.<sup>35</sup> In our metal-dielectric nanostructures two kinds of CT processes can be foreseen: i) electron transition from the R6G HOMO excited to the LUMO by the impinging light and then injected into TiO<sub>2</sub> conduction band; ii) electron transition from the TiO<sub>2</sub> valence band towards the surface states lying in the titania gap induced by the exciting light and a successive electron injection into the LUMO of the adsorbed R6G.<sup>48</sup> Raman spectra of R6G incubated in bare TiO<sub>2</sub> NTs are reported in Figure S2a. Without the Ag coating R6G at low molar concentration cannot be detected. However, R6G impregnated TiO<sub>2</sub> NTs show a very low fluorescence intensity (see as a comparison the spectra of R6G on bare crystalline silicon, Figure S2b). Such a fluorescence quenching can be actually ascribed to the CT processes discussed before, activating non-radiative recombinations.

The synergy between CT (before discussed in terms of electron transitions involving the TiO<sub>2</sub> surface states/conduction band vs. the R6G LUMO level) and EM enhancement (ascribed to the LSP resonances experimentally checked by reflectance measurements) could justify the lowest LOD obtained in SERRS regime, which is compatible with a single molecule detection.<sup>46</sup> Microfluidic devices coupled with SERS detection methods attracted attention for the possibility to integrate a biological

or chemical protocol and a very sensitive technique. In addition to this, microfluidics can solve problems dealing with a non-uniform molecule distribution (i.e. "coffee ring" effects, where molecules likely accumulate on the edge of the liquid droplets<sup>49</sup>). Actually, a microfluidic circuitry can better confine the liquid analyte close to the SERS-active area, also during an eventual evaporation process. Moreover, a microfluidic platform can be optimized in order to reduce the reagents volume, decreasing the analysis cost. Finally, optofluidic devices based on elastomeric matrices such as PDMS, have also noticeable advantages in their flexibility to conform to the underlying object as they can be wrapped onto curved surfaces and can be easily cut into different shapes and sizes. One of the main issue in coupling a PDMS cover with a nanostructured surface is related to the substrate wettability. As discussed above (see Figure 4b) the 30s Ag sputtered substrate showed a limited hydrophobicity, and consequently it can take advantages in terms of surface wetting by aqueous solutions from the physical confinement produced by the integration into a microfluidic device. For the longer  $t_{\text{SPT}}$  samples, a surface wetting control is worthless. Moreover, since the 30s Ag coated sample correspond to the most performant SERS substrate, it was chosen for microfluidic integration.

A PDMS-based microfluidic device was fabricated as described in the experimental section (see also Figure S1 in ESI) and the SERS measurements were performed using a long working distance objective to focus/collect the exciting/scattered light on the Ag-TiO<sub>2</sub> NT surface (backscattering configuration). Figure 7a shows the SERS spectra of R6G injected into the microfluidic channel on a 30s Ag sputtered TiO<sub>2</sub> NT substrate. The device shows a good uniformity of the Raman signal along the microchannel with a moderate Raman intensity fluctuation. We calculated a relative standard deviation of the Raman intensity of 16% over 1 mm of linear scanning (analyzing the band of C-C stretching in xanthene ring at  $1610\text{ cm}^{-1}$ , after a baseline subtraction).

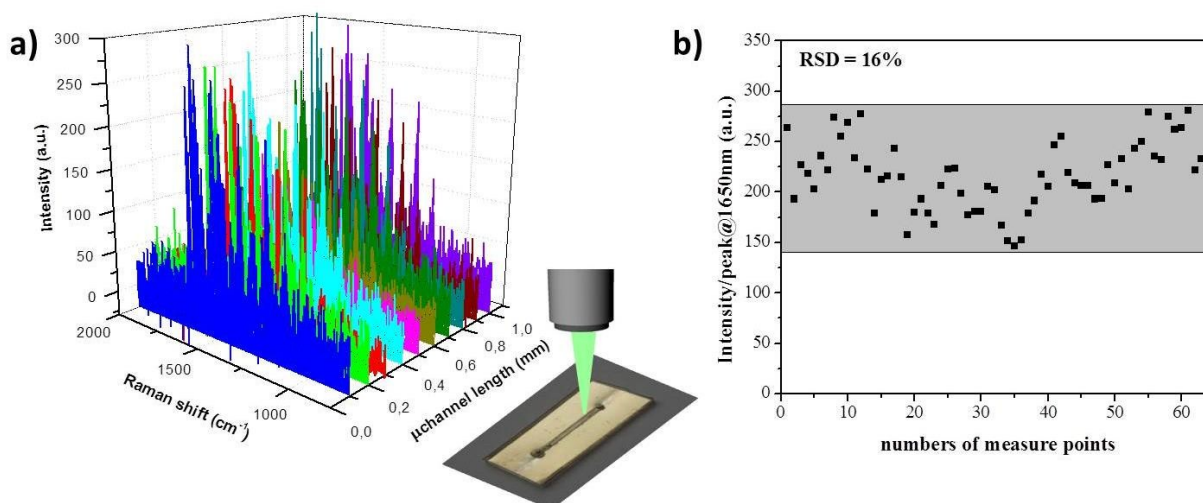
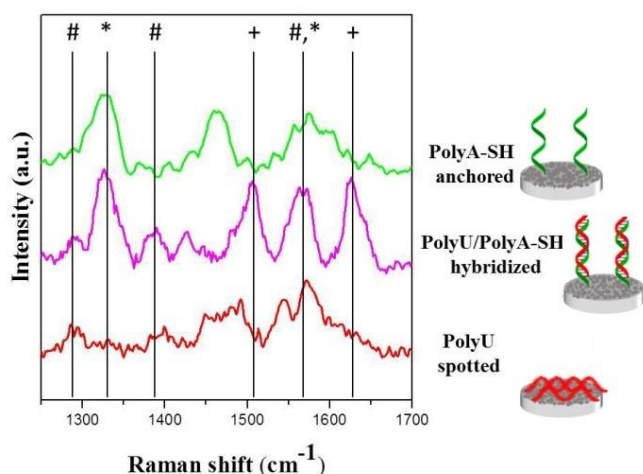


Figure 7. SERS spectra of R6G at  $10^{-6}\text{ M}$  (a) and peak intensity at  $1650\text{ cm}^{-1}$  of R6G along the microfluidic channel (b).

As a check of the optofluidic device performance, we measured the Raman intensity fluctuation of the  $1610\text{ cm}^{-1}$  band on a free surface of silvered  $\text{TiO}_2$  NTs (without any fluidic integration), calculating a relative standard deviation of 31% over the same scanning length. This result can be considered as a proof of the advantages offered by the microfluidics, in agreement with uniformity analysis recently published on other SERS platforms.<sup>49-52</sup>

In order to test the potentiality of the discussed SERS platform, the immobilization of a model alkylthiol-capped DNA oligo strand (SH-C6-AAAAAA, PolyA-SH) on silvered  $\text{TiO}_2$  NTs, and the hybridization of its complementary miRNA sequence (UUUUUUU, PolyU), is reported.

The first part of the protocol, described in the experimental section, allows to bind the thiolated termination of PolyA-SH to the silver nanoparticles at  $\text{TiO}_2$  NTs (sample with  $t_{\text{sputt}}=30\text{s}$  that has the lower LOD for R6G in resonant condition). SERS spectrum of PolyA-SH chemisorbed on silver nanoparticles is mainly influenced by the presence of purine and presents three principal bands (Figure 8) related to C-N stretching at  $1329\text{ cm}^{-1}$ , C=N stretching at  $1464\text{ cm}^{-1}$  and ring stretching of adenine at  $1567\text{ cm}^{-1}$ .<sup>53-55</sup>



**Figure 8.** SERS spectra of polyA-SH immobilized on Ag nanoparticle surface and after hybridization event with polyU. Spectrum of polyU spotted on silver nanoparticles is shown for comparison. Black lines report the fingerprint of polyU (#), polyA-SH (\*) and complex form (+) present in polyU/PolyA-SH hybridized spectrum.

After the formation of PolyA-SH monolayer and the removal of unbound DNA by washing, a PolyU solution was spotted and incubated to allow the hybridization. A spectrum was collected after having washed the sample to remove unspecific RNA bound. The complex made up by PolyA-SH and PolyU has typical features related to DNA sequence ( $1329\text{ cm}^{-1}$ ,  $1567\text{ cm}^{-1}$

$1610\text{ cm}^{-1}$ ), to miRNA strand ( $1290\text{ cm}^{-1}$ ,  $1380\text{ cm}^{-1}$ ,  $1567\text{ cm}^{-1}$ ) and to the change in the orientation and conformation due to hybridization event ( $1503\text{ cm}^{-1}$ ,  $1647\text{ cm}^{-1}$ ). The bands of PolyU are dominated by pyrimidine mode at  $1290\text{ cm}^{-1}$  (ring stretching), at  $1380\text{ cm}^{-1}$  (C-N stretching),  $1567\text{ cm}^{-1}$  (ring stretching) and by ribose OH group deformation at around  $1460\text{ cm}^{-1}$ <sup>56,57</sup> which disappears when the miRNA-DNA complex is formed. The peaks at  $1503\text{ cm}^{-1}$  and  $1647\text{ cm}^{-1}$  in the hybridization complex can be ascribed to  $\text{NH}_2$  deformation and scissoring modes in adenine, respectively.<sup>53,55</sup> These features and the presence of polyA-SH and polyU bands confirm that the hybridization has taken place.

## Conclusions

In summary, Ag NPs were grown by d.c. sputtering on  $\text{TiO}_2$  nanotube arrays by anodic oxidation of Ti foils. We investigated the Ag NPs morphology on the  $\text{TiO}_2$  NTs substrates aimed to optimize the SERS enhancement in the metal-dielectric nanostructures. The structure characterized by a plasmonic resonance matching with the excitation showed a remarkable R6G limit of detection down to  $10^{-14}\text{ M}$ . Good homogeneity of the SERS signal was found for the optimized substrate integrated into a PDMS microfluidic device, with a low intensity fluctuation along the fluidic microchannel.

Lastly, the biosensing performance of Ag- $\text{TiO}_2$  NT based optofluidic device was tested exploiting an optimized protocol for the oligonucleotides probes immobilization on the metal-dielectric surfaces, reporting the Raman detection of a model alkylthiol-capped DNA oligo strand and the hybridization of its complementary sequence.

The experimental results showed that these substrates are characterized by high sensitivity and uniformity, which make them, besides other recently proposed SERS platforms<sup>58,59</sup>, promising for multiple detection of different molecular species. Moreover they are cost-effective, robust and adaptable to several different environments and target analytes.

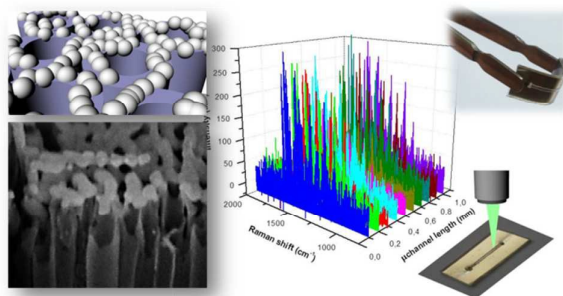
## Acknowledgements

This research has received funding from the Italian Flagship Project NANOMAX and the FIRB NEWTON.

## Notes and references

- 1 K. Kneipp, H. Kneipp, I. Itzkan, R. R. Dasari and M. S. Feld, *J. Phys. Condens. Matter.*, 2002, **14**, R597.

- 2 T. M. Herne, A. M. Ahern and R. L. Garrell, *J. Am. Chem. Soc.*, 1991, **113**, 846.
- 3 A. S. D. S. Indrasekara, S. Meyers, S. Shubeita, L. C. Feldman, T. Gustafsson and L. Fabris, *Nanoscale*, 2014, **6**, 8891.
- 4 A. Weiss and G. Haran, *J. Phys. Chem. B*, 2001, **105**, 12348.
- 5 L. Chuntunov and G. Haran, *Nano Lett.*, 2011, **11**, 2440–2445.
- 6 T. Itoh, M. Iga, H. Tamaru, K. Yoshida, V. Biju and M. Ishikawa, *J. Chem. Phys.*, 2012, **136**, 24703.
- 7 L. Gunnarsson, E. J. Bjerneld, H. Xu, S. Petronis, B. Kasemo and M. Käll, *Appl. Phys. Lett.* 2001, **78**, 802.
- 8 U. Huebner, R. Boucher, H. Schneidewind, D. Cialla and J. Popp, *Microelectron. Eng.*, 2008, **85**, 1792.
- 9 H. X. Xu, J. Aizpurua, M. Kall and P. Apell, *Phys. Rev. E*, 2000, **62**, 4318.
- 10 A. Otto, I. Mrozek, H. Grabhorn and W. Akemann, *J. Phys.: Condens. Matter*, 1992, **4**, 1143.
- 11 W. H. Park and Z. H. Kim, *Nano Lett.*, 2010, **10**, 4040.
- 12 S. Nie and S. R. Emory, *Science*, 1997, **275**, 1102.
- 13 K. Kneipp, Y. Wang, H. Kneipp, L. T. Perelman, I. Itzkan, R. R. Dasari and M. S. Feld, *Phys. Rev. Lett.*, 1997, **78**, 1667.
- 14 X. Wang, W. Shi, G. She and L. Mu, *Phys. Chem. Chem. Phys.*, 2012, **14**, 5891.
- 15 S. Hayashi, R. Koh, Y. Ichiyama and K. Yamamoto, *Phys. Rev. Lett.*, 1988, **60**, 1085.
- 16 L. G. Quagliano, *J. Am. Chem. Soc.*, 2004, **126**, 7393.
- 17 X. T. Wang, W. S. Shi, G. W. She and L. X. Mu, *J. Am. Chem. Soc.*, 2011, **133**, 16518.
- 18 Y. Wang, W. Ruan, J. Zhang, B. Yang, W. Xu, B. Zhao and J. R. Lombardi, *J. Raman Spectrosc.*, 2009, **40**, 1072.
- 19 B. H. Loo, *J. Electroanal. Chem.*, 1982, **136**, 209.
- 20 A. Kudelski, W. Grochala, M. Janik-Czachor, J. Bukowska, A. Szummer and M. Dolata, *J. Raman Spectrosc.*, 1998, **29**, 431.
- 21 H. Yamada and Y. Yamamoto, *Surf. Sci.*, 1983, **134**, 71.
- 22 A. Lamberti (2015), Metal-Oxide Nanostructures for Surface Enhanced Raman Spectroscopy, submitted to *Encyclopedia of Nanotechnology*, Springer
- 23 I. Alessandri, *J. Am. Chem. Soc.*, 2013, **135**, 5541.
- 24 Y. F. Chan, H. J. Xu, L. Cao, Y. Tang, and X. M. Sun, *J. Appl. Phys.*, 2012, **111**, 033104.
- 25 T. Sakano, Y. Tanaka, R. Nishimura, N. N. Nedyalkov, P. A. Atanasov, T. Saiki and M. Obara, *Journal of Physics D: Applied Physics*, 2008, **41**, 235304.
- 26 H. Tang, G. Meng, Q. Huang, Z. Zhang, Z. Huang and C. Zhu, *Adv. Funct. Mater.*, 2012, **22**, 218.
- 27 M. A. Khan, T. P. Hogan and B. Shanker, *J. Raman Spectrosc.*, 2009, **40**, 1539.
- 28 N. Ji, W. Ruan, C. Wang, Z. Lu and B. Zhao, *Langmuir*, 2009, **25**, 11869.
- 29 W. Song, Y. Wang and B. Zhao, *J. Phys. Chem. C*, 2007, **111**, 12786.
- 30 Z. Bao, X. Liu, J. Dai, Y. Wu, Y. H. Tsang and D. Y. Lei, *Appl. Surf. Sci.*, 2014, **301**, 351.
- 31 X. Li, G. Chen, L. Yang, Z. Jin and J. Liu, *Adv. Funct. Mater.*, 2010, **20**, 2815.
- 32 Y. Xie, Y. Jin, Y. Zhou and Y. Wang, *Appl. Surf. Sci.*, **313**, 2014, 549.
- 33 A. Lamberti, A. Sacco, S. Bianco, M. Quaglio, D. Manfredi and C. F. Pirri, *Microelectron. Eng.*, 2013, **111**, 137.
- 34 D. Pugliese, A. Lamberti, F. Bella, A. Sacco, S. Bianco and E. Tresso, *Org. Electron.*, 2014, **15**, 3715.
- 35 A. Lamberti, N. Garino, A. Sacco, S. Bianco, A. Chiodoni and C. Gerbaldi, *Electrochim. Acta*, 2015, **151**, 222.
- 36 A. Lamberti, S. L. Marasso and M. Cocuzza, *RSC Adv.*, 2014, **4**, 61415.
- 37 A. Lamberti, A. Sacco, S. Bianco, D. Manfredi, M. Armandi, M. Quaglio, E. Tresso, C. F. Pirri, *Solar Energy*, 2013, **95**, 90.
- 38 A. Lamberti, A. Sacco, S. Bianco, D. Manfredi, F. Cappelluti, S. Hernandez, M. Quaglio, C. F. Pirri, *Phys. Chem. Chem. Phys.*, 2013, **15**, 2596.
- 39 A. Lamberti, A. Chiodoni, N. Shahzad, S. Bianco, M. Quaglio and C. F. Pirri, *Scientific Reports*, 2015, **5**.
- 40 A. Virga, P. Rivolo, E. Descrovi, A. Chiolerio, G. Digregorio, F. Frascella, M. Soster, F. Bussolino, S. Marchiò, F. Geobaldo and F. Giorgis, *J. Raman Spectrosc.*, 2012, **43**, 730.
- 41 A. Lamberti et al., *J. Phys. Chem. B*, submitted 2015
- 42 H. Mertens, J. Verhoeven, A. Polman and F. D. Tichelaar, *Appl. Phys. Lett.*, 2004, **85**, 1317; A. Virga, R. Gazia, L. Pallavidino, P. Mandracci, E. Descrovi, A. Chiodoni, F. Geobaldo and F. Giorgis, *Phys. Status Solidi C*, 2010, **7**, 1196.
- 43 S.-H. Uhm, D.-H. Song, J.-S. Kwon, S.-B. Lee, J.-G. Han and K.-N. Kim, *J. Biomed. Mater. Res. Part B Appl. Biomater*, 2014, **102B**, 592.
- 44 T. Vosgröne, A. J. Meixner, *Chem. Phys. Chem.*, 2005, **6**, 154.
- 45 Y. Q. Wang, S. Maa, Q. Q. Yanga and X. J. Li, *Appl. Surf. Science*, 2012, **258**, 5881..
- 46 A. Virga, P. Rivolo, F. Frascella, A. Angelini, E. Descrovi, F. Geobaldo and F. Giorgis, *J. Phys. Chem. C*, 2013, **117**, 20139.
- 47 V. Likodimos, T. Stergiopoulos, P. Falaras, J. Kunze and P. Schmuki, *J. Phys. Chem. C*, 2008, **112**, 12687.
- 48 L. Yang, X. Jiang, W. Ruan, B. Zhao, W. Xu and J.R. Lombardi, *J. Phys. Chem. C*, 2008, **112**, 20095.
- 49 A. Lamberti, A. Virga, A. Angelini, A. Ricci, E. Descrovi, M. Cocuzza and F. Giorgis, *RSC Adv.*, 2015, **5**, 4404.
- 50 X.-M. Lin, Y. Cui, Y.-H. Xu, B. Ren and Z.-Q. Tian, *Anal. Bioanal. Chem.*, 2009, **394**, 1729.
- 51 M. A. Khan, T. P. Hogan and B. Shanker, *J. Raman Spectrosc.*, 2009, **40**, 153940
- 52 Driskell, S. Shanmukh, Y. Liu, S. B. Chaney, X. J. Tang, Y. P. Zhao and R. A. Dluhy, *J. Phys. Chem. C*, 2008, **112**, 89512.
- 53 O. M. Primera-Pedrozoa, G. Del Mar Rodríguez, J. Castellanos, H. Felix-Riveraa, O. Restob and S. P. Hernández-Riveraa, *Spectrochimica Acta Part A: Molecular and Biomolecular Spectroscopy*, 2012, **87**, 77.
- 54 S. E. J. Bell and N. M. S. Sirimuthu, *J. Am. Chem. Soc.*, 2006, **128**, 15580.
- 55 B. Giese and D. McNaughton, *J. Phys. Chem. B*, 2002, **106**, 101.
- 56 S. Miljanić, A. Dijanošić and I. Matić, *Spectrochimica Acta Part A: Molecular Spectroscopy*, 2015, **137**, 1357.
- 57 K.-H. Choa, J. Choob and S.-W. Joo, *Spectrochimica Acta Part A: Molecular Spectroscopy*, 2005, **61**, 1141.
- 58 H. Liu, Z. Yang, L. Meng, Y. Sun, J. Wang, L. Yang, J. Liu, and Z. Tian, *J. Am. Chem. Soc.*, 2014, **136**, 5332.
- 59 L. Yang, P. Li and J. Liu, *RSC Adv.*, 2014, **4**, 49635.



A novel SERS optofluidic sensor based on Ag-decorated TiO<sub>2</sub> nanotubes has been developed for repeatable detection of organic molecules and biological assays.